Geochemistry Geophysics Geosystems G3

Article
Volume 15, Number 1
31 January 2014
doi: 10.1002/2013GC005018
ISSN: 1525-2027

Published by AGU and the Geochemical Society

Critical taper analysis reveals lithological control of variations in detachment strength: An analysis of the Alpine basal detachment (Swiss Alps)

C. von Hagke
Department of Geological and Planetary Sciences, California Institute of Technology, 1200 E California Boulevard, Pasadena, California 91106, USA (vonhagke@caltech.edu)

O. Oncken
Department of Lithosphere Dynamics, Helmholtz Centre Potsdam, GFZ, German Research Centre for Geosciences, Potsdam, Germany

S. Evseev
Geologisches Institut, Freie Universitaet Berlin, Berlin, Germany

[1] Although evidence for weak detachments underlying foreland thrust belts exists, very little is known about the lateral variations in effective strength, as well as the geological nature of such variations. Using critical taper analysis, we show that a detailed and systematic measurement of surface slope of the Central European Alps reveals variations in strength parameter F along the detachment, based on the argument that the Alps are close to the critical state. We show that the basal detachment is very weak near the deformation front but strengthens toward the hinterland. Very low F (effective coefficient of friction plus normalized cohesion) values of <0.1 and even 0.05 occur within evaporites and within shales in Triassic (west) or Upper Cretaceous/Lower Tertiary sequences (east) used by the Alpine sole detachment. These very low values in shales—comparably low values are reported from other orogens—are caused partly by slightly elevated pore pressures ($\lambda > 0.54$) but may also require additional mechanisms of dynamic weakening.

Components: 11,218 words, 7 figures.

Keywords: critical taper; central Alps; detachment strength; wedge.

Index Terms: 8011 Kinematics of crustal and mantle deformation: Structural Geology; 8034 Rheology and friction of fault zones: Structural Geology; 8015 Local crustal structure: Structural Geology; 8104 Continental margins: convergent: Tectonophysics; 8163 Rheology and friction of fault zones: Tectonophysics; 9335 Europe: Geographic Location.

Received 29 August 2013; **Revised** 12 November 2013; **Accepted** 24 November 2013; **Published** 31 January 2014.

von Hagke, C., O. Oncken, and S. Evseev (2014), Critical taper analysis reveals lithological control of variations in detachment strength: An analysis of the Alpine basal detachment (Swiss Alps), *Geochem. Geophys. Geosyst.*, *15*, 176–191, doi:10.1002/2013GC005018.

1. Introduction

[2] Basal detachments beneath active thrust wedges may be extremely weak [e.g., *Suppe*, 2007; *Ruh et al*., 2012]. The strength of such a basal detachment is usually estimated using various strategies based on critical wedge theory [*Davis et al*., 1983; *Dahlen et al*., 1984; *Dahlen*, 1990] as well as from numerical analysis [*Cubas et al*., 2013]. Several studies have shown that it is

possible to estimate the coefficient of basal friction by applying mechanical models of wedges. *Davis and von Huene* [1987] apply the critical Coulomb wedge model [*Dahlen et al*., 1984] using the hanging wall fault geometry at the Aleutian Trench and infer a weak detachment, which they ascribed to elevated pore pressure. *Schott and Koyi* [2001] use an elastic wedge model [*Yin*, 1993; *Mandal et al*., 1997] and calculate the coefficient of basal friction for the Makran and Nankai wedges from fault geometry and material properties and find values of $\mu_b = 0.16$ and 0.2, respectively, which is extremely low. Furthermore, detachment strength variations along and across strike have been reported from various orogens and analyzed in sandbox and numerical models [e.g., *Calassou et al*., 1993; *Baby et al*., 1995; *Macedo et al*., 1999; *Schreurs et al*., 2001; *Calais et al*., 2002; *Couzens-Schultz et al*., 2003; *Bose et al*., 2009]. These studies focus on a (both, transient or sharp) change from brittle to ductile behavior, but little is known about strength variations within a single brittle detachment. In particular, the regional variability of the increasingly reported low strength values or their relationship with detachment lithology remain largely unconstrained.

[3] Recently, *Suppe* [2007], extending the original approach of *Dahlen* [1990] used the example of the Taiwan wedge and the toe of the Niger delta to show that it is possible to constrain detachment strength (the magnitude of detachment strength parameters, respectively, see below) by a simple measurement of surface and detachment slope (e.g., see also application of this strategy to the Central Andes foreland belt by *Oncken et al*. [2012]). In this study, we closely follow this approach and show that the equations Suppe has derived can be used to reveal strength parameter variations along one single brittle detachment. To this end, we carry out a detailed analysis of wedge topography and the shape of the basal detachment, assuming that the equations that *Suppe* [2007] derived for the entire wedge are also valid for every point within the wedge. Before this analysis, we must address this assumption. Analogue experiments and numerical studies show that the basis of critical taper theory, which is failure equilibrium throughout the wedge, is violated if deformation in elastic-plastic materials is localized due to strain weakening [*Lohrmann et al*., 2003; *Simpson*, 2011]. Accordingly, in order to obtain meaningful results, geometric detail of spatial detachment strength variations is limited by the spacing of the strain-weakening parts, i.e., to the thrust spacing of the fold and thrust belt forming the overlying wedge.

[4] The European Alps provide a suitable example to investigate variations in detachment strength in a natural system because of the availability of high-resolution geologic and tectonic maps for the entire orogen. Additionally, various orogen-scale cross sections provide control on the 3-D architecture and the depth of the detachment horizons, their stratigraphic position and lithologies involved [e.g., *Schmid et al*., 1996; *Escher and Beaumont*, 1997; *Pfiffner et al*., 1997b; *Burkhard and Sommaruga*, 1998; *Schmid et al*., 2004; *Lüschen et al*., 2006; *Lammerer et al*., 2008; *Pfiffner*, 2010]. The focus of this study is the central part of the orogen where along strike variations in deep structure and timing of metamorphic events are small enough to suggest along strike consistency of wedge dynamics [e.g., *Gebauer*, 1999; *Thöny*, 1999; *Schmid and Kissling*, 2000; *Schmid et al*., 2004].

2. Geological Framework

[5] The Central European Alps are the result of convergence and collision of the Adria and European plates [e.g., *Trümpy*, 1960; *Frisch*, 1979; *Stampfli et al*., 2001; *Schmid et al*., 2004]. Following southward subduction of the Penninic Ocean, the continents collided at ~35 Ma, [e.g., *Schmid et al*., 1996]. On-going convergence resulted in northward thrusting of the European passive margin (Helvetics) and downward flexing of the European Plate. This entailed the formation of the North Alpine Foreland Basin and the subsequent deposition of two regressive cycles of marine and fresh water sediments [e.g., *Pfiffner*, 1986; *Sinclair and Allen*, 1992; *Schlunegger et al*., 1997; *Sinclair*, 1997; *Kempf et al*., 1999; *Berger et al*., 2005; *Willett and Schlunegger*, 2010]. The southern part of the foreland basin was folded and thrusted shortly after deposition, and today forms the Subalpine Molasse [*Homewood et al*., 1986]. After ~10 Ma, folding of the Jura Mountains started due to detachment of foreland sediments along Triassic evaporites [*Buxtorf*, 1907, 1916; *Laubscher*, 1961, 1977; *Bollinger et al*., 1993]. The Jura Mountains form now, together with the North Alpine Foreland Basin, the external part of the Alpine chain [e.g., *Burkhard*, 1990; *Burkhard and Sommaruga*, 1998]. Shortening within the Subalpine Molasse and Jura Mountains is transferred southward to below the External Massifs

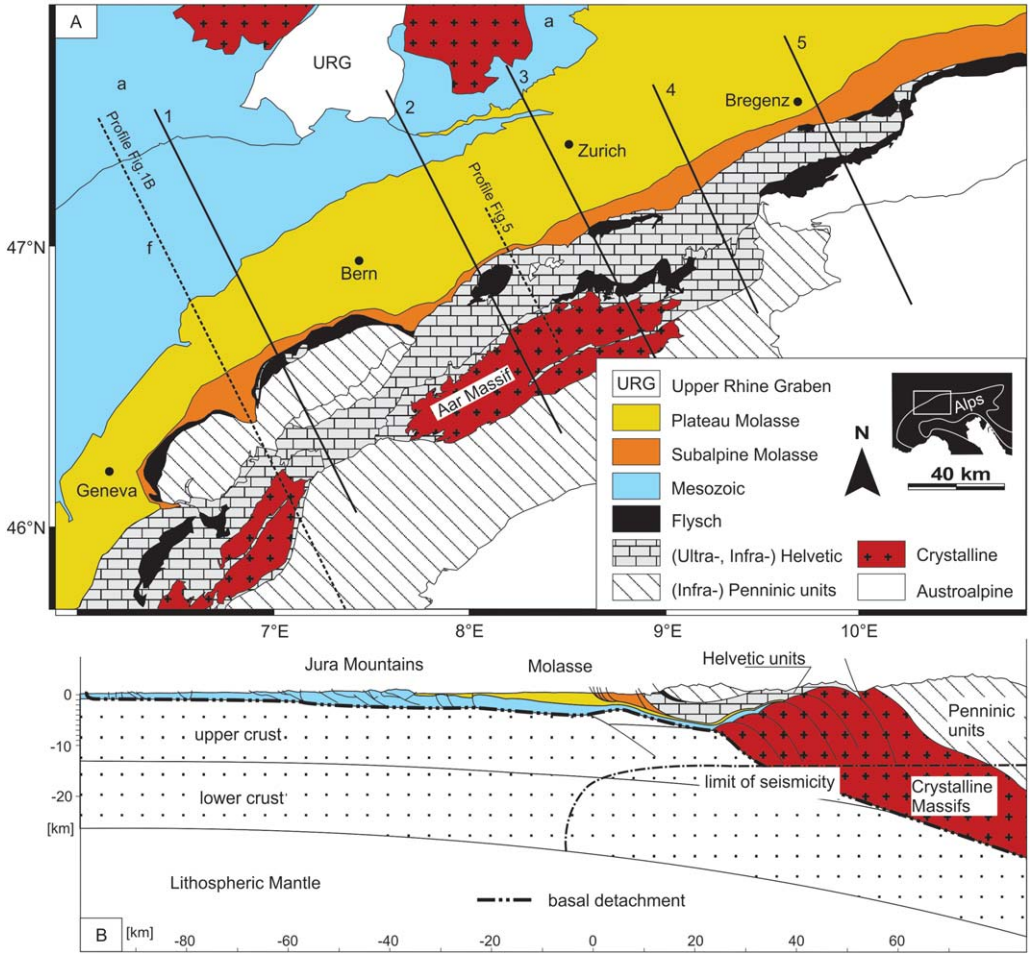

Figure 1. a. Tectonic map of the Northern Central Alps and the adjacent foreland based on *Spicher* [1980] and *Schmid et al*. [2004]. a—autochthonous Jura, f—folded Jura, traces of analyzed profiles indicated by black lines (1–5). Note the crystalline bodies within the Alps, the External Massifs (including the Aar Massif). Figure 1b is a cross section through the Central Alps, highlighting the major tectonic units and the basal detachment (modified after *Burkhard and Sommaruga* [1998]). Tectonic units discussed in the text are colored. Limit of seismicity (coinciding with the 300–350°C isotherm) based on *Okaya et al*. [1996].

[*Boyer and Elliott*, 1982; *Laubscher*, 1986; *Burkhard*, 1990; *Escher and Beaumont*, 1997; *Pfiffner et al*., 1997a]. The latter consist of accreted European basement now overlying the recent Alpine basal detachment, and today form the northern drainage divide of the Central Alps (Figure 1). Several studies have pointed out the linkage of exhumation of the Aar and Gotthard Massifs with folding and thrusting within the Subalpine Molasse and the Jura Mountains, which allows considering the entire suite of tectonic units from the External Massifs through the Subalpine Molasse and Jura Mountains as part of a single orogenic wedge [*Boyer and Elliott*, 1982; *Burkhard*, 1990; *Pfiffner et al*., 1990; *Pfiffner et al*., 1997b; *Burkhard and Sommaruga*, 1998; *Fügenschuh and Schmid*, 2003; *von Hagke et al*., 2012], (Figure 1b).

[6] The critical taper theory, derived from force balance considerations, predicts that a wedge will evolve toward failure equilibrium (the critical state) characterized by being at the verge of brittle failure internally and at its base. Force balance means that the detachment parallel component of gravitational body force and the resulting overburden pressure, together with basal shear traction equal compressive push [*Davis et al*., 1983]. Hence, a central requirement for applying wedge theory to deduce mechanical properties is that the system is near failure equilibrium at the minimum or maximum critical condition, which we will

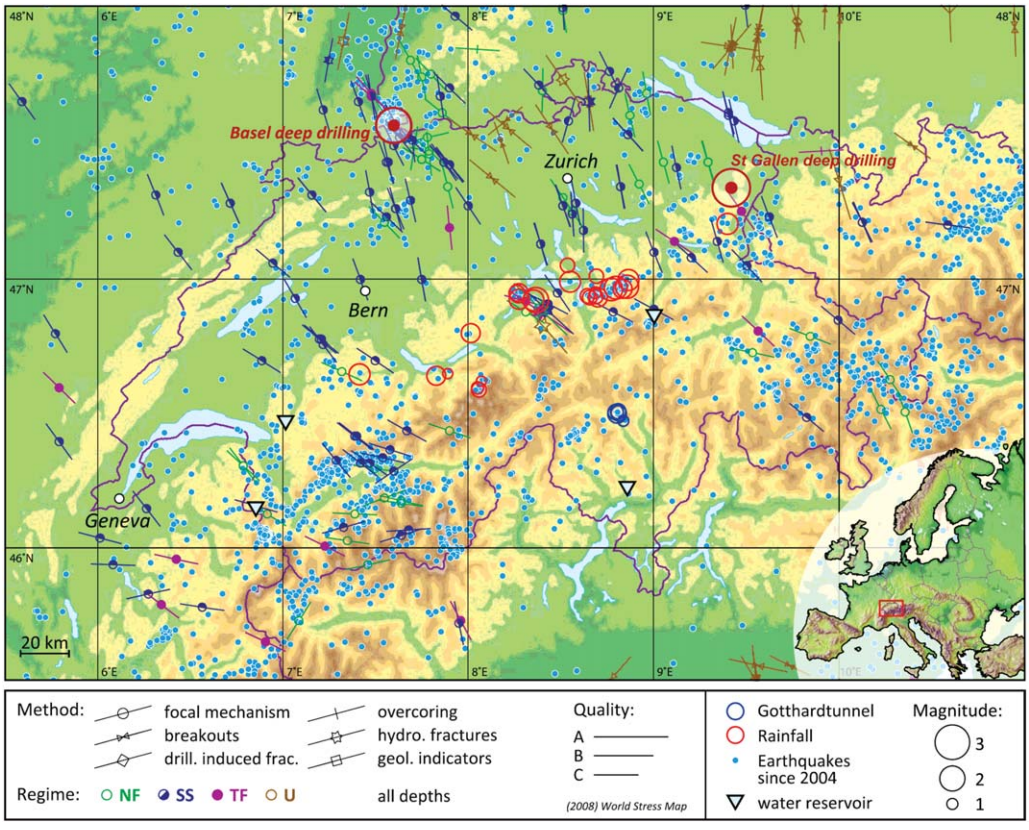

Figure 2. Seismic activity in the Central Alps shows some clustering, but is generally distributed all over the orogen (note for instance the seismic cluster of the glacially oversteepened Rhone Valley). For optical clarity, we chose the arbitrary interval from 2004 to 2009 from the SED catalogue [*Fäh et al*., 2011]. Blue dots represent the respective epicenters, not magnitude. Seismic events triggered by rainfall, drilling of the Gotthard Tunnel, and geothermal deep drillings are indicated as circles that scale with magnitude. Water reservoirs that triggered earthquake swarms are represented by blue triangles. Stress indicators are taken from the World Stress Map [*Heidbach et al*., 2008].

address below. Equilibrium, accordingly, should be reflected by a self-similarly growing wedge with a stable surface taper (α) and detachment dip (β) over time (critical wedge theory is time independent, see equation (1)) [*Davis et al*., 1983; *Dahlen*, 1984; *Dahlen et al*., 1984]. Such a critical wedge should react instantaneously to changes in stress regime. For instance, the Taiwan fold and thrust belt, a classic example of critical wedge, has been shown to react with internal deformation only because of air pressure lowering due to seasonal typhoons [*Liu et al*., 2009]. Extending this conventional application of wedge theory, *Simpson* [2011] has shown in a more detailed numerical study that substantial parts of a thrust wedge—i.e., major parts of thrust sheets or imbricates separated by the thrusts—may be in a different stress state well below failure. Over time, such wedges tend to evolve toward a taper near the minimum critical condition that is predicted by wedge theory, although wedge theory does not explicitly include the role of weak faults and strain localization.

[7] The Alps provide an exceptional data set to observe whether, and at which scale, they are at the verge of failure: in addition to natural phenomena, human impact and resulting disturbances of the stress field is abundant and distributed across the entire mountain range (Figure 2). In many regions of the Alps, water reservoir impoundment induced seismic activity. Famous examples in the Central and Western Alps are Monteynard, France, where an earthquake of magnitude M_L 4.9 was triggered shortly after filling a reservoir [*Rothé*, 1970; *Gupta et al*., 1972], the Lake of Salanfe, Switzerland, where abnormally high seismicity after reservoir filling triggered thermal springs at a distance of ~15 km [*Bianchetti et al*., 1992], and the Verzasca Dam, Switzerland, where several hundred local earthquakes occurred after filling [*Süsstrunk*, 1968;

Gupta et al., 1972]. A few events have been attributed to the Swiss dams of Linth-Limmern and Lac Hongrin [*Fäh et al*., 2011]. Drilling of the Gotthard Base Tunnel in the Central Alps triggered a series of 112 earthquakes with a maximum magnitude of M_L 2.4 [*Husen et al*., 2012]. Fluid injection in a geothermal drilling in Basel stimulated several thousand earthquakes in 2006 and 2007 with a maximum magnitude of M_L 3.4 [*Häring et al*., 2008; *Deichmann and Ernst*, 2009; *Ripperger et al*., 2009; *Bachmann et al*., 2011]. On 20 July 2013, the Swiss Seismological Service registered a M_L 3.6 earthquake, related to stimulation activities in the St. Gallen geothermal borehole (www.seismo.ethz.ch/index_EN), which likewise was accompanied by more than 500 smaller quakes (as of 23 July 2013). (For location of the Basel and St Gallen deep drillings see Figure 2.) In addition, rainfall and resulting variations in water table caused seismic activity in the Central Alps. *Deichmann et al*. [2006] and *Husen et al*. [2007] show that a heavy rainfall event in 2005 caused abnormally high seismicity and *Roth et al*. [1992] sees correlation between intense precipitation coupled with seasonal snow melt and shallow seismicity in the eastern Swiss Alps. Besides these transient effects, seismicity in the Central Alps and their north-western foreland is extensive and also found in regions between major active structures (Figure 2). Moreover, the fan shape of the maximum horizontal stresses transverse to the Alpine arc exhibits an identical, strike-slip dominated, kinematic pattern within the orogen as well as in its foreland within the area of interest [*Sue et al*., 2007; *Heidbach et al*., 2008]. Both latter observations indicate active deformation beyond the above-described local response to perturbations. In sum, this suggests that a very substantial portion of the Central Alpine wedge is close to failure equilibrium and that it has largely evolved toward the minimum critical condition during ongoing deformation.

[8] To apply the critical taper theory, i.e., to accommodate the assumption of failure equilibrium, the basal detachment must also be at the verge of failure. This appears probable, as the foreland is seismically active above and below the detachment horizon [*Fäh et al*., 2011]. In addition, the mean of the measured maximum horizontal stress orientations (S_H) above and below the detachment is identical within statistical error [*Deichmann and Marschall*, 2002; *Kastrup et al*., 2004; *Valley and Evans*, 2009; *Deichmann*, 2010; *Heidbach and Reinecker*, 2012]. In the eastern Central Alps, neo-tectonic activity shows that the basal detachment is still active [*Persaud and Pfiffner*, 2004; *Fäh et al*., 2012]. In the western Alps, *Mosar* [1999] has argued for a newly developing midcrustal detachment underneath the Molasse Basin [see also *Lacombe and Mouthereau*, 2002] and a change from thin to thick-skinned tectonics in the Jura Mountains [*Giamboni et al*., 2004; *Madritsch et al*., 2008]. However, this midcrustal detachment is only incipient and has probably not yet developed into a through-going tabular fault able to modify and control surface taper [*Mosar*, 1999]. We, therefore, do not consider it to be relevant for present-day wedge dynamics. In any case, development of such a new detachment requires active shortening, which is corroborated by active convergence in the Jura Mountains [*Madritsch et al*., 2010]. Hence, the basal detachment is likely creeping or close to the verge of failure too.

3. Critical Taper Analysis

[9] In a mechanically homogeneous wedge, the critical taper equation using the small angle approximation of *Dahlen* [1990] is

$$(\alpha+\beta) \approx \frac{(1-\rho_f/\rho)\beta+\mu_b(1-\lambda_b)+S_b/\rho gH}{(1-\rho_f/\rho)+2(1-\lambda)\left(\frac{\sin\phi}{1-\sin\phi}\right)+C/\rho gH} \quad (1)$$

where ρ_f is the density of the fluid above the wedge (water or air), ρ is the mean density of rock, μ_b is the basal friction coefficient, λ_b is the basal pore fluid to lithostatic pressure ratio, S_b is basal cohesion, C is compressive wedge strength, ϕ is the angle of internal friction, and H is wedge thickness. In simple terms, the critical taper angle ($\alpha + \beta$) is dependent on the ratio of basal fault strength and wedge internal strength. *Suppe* [2007] collects all wedge-strength terms into one value (W) and all fault strength terms into one value (F) and reorganizes the critical taper equation to

$$F=\alpha(1-\rho_f/\rho)+(\alpha+\beta)W \quad (2)$$

[10] As the Central Alps are a subaerial wedge, ρ_f/ρ (air density over rock density) will be negligible and it is possible to substitute $(1-\rho_f/\rho) \cong 1$ [*Suppe*, 2007] and write for the Central Alps

$$F=\alpha+(\alpha+\beta)W \quad (3)$$

[11] W is a dimensionless parameter, assessing wedge-strength independent of the amount of

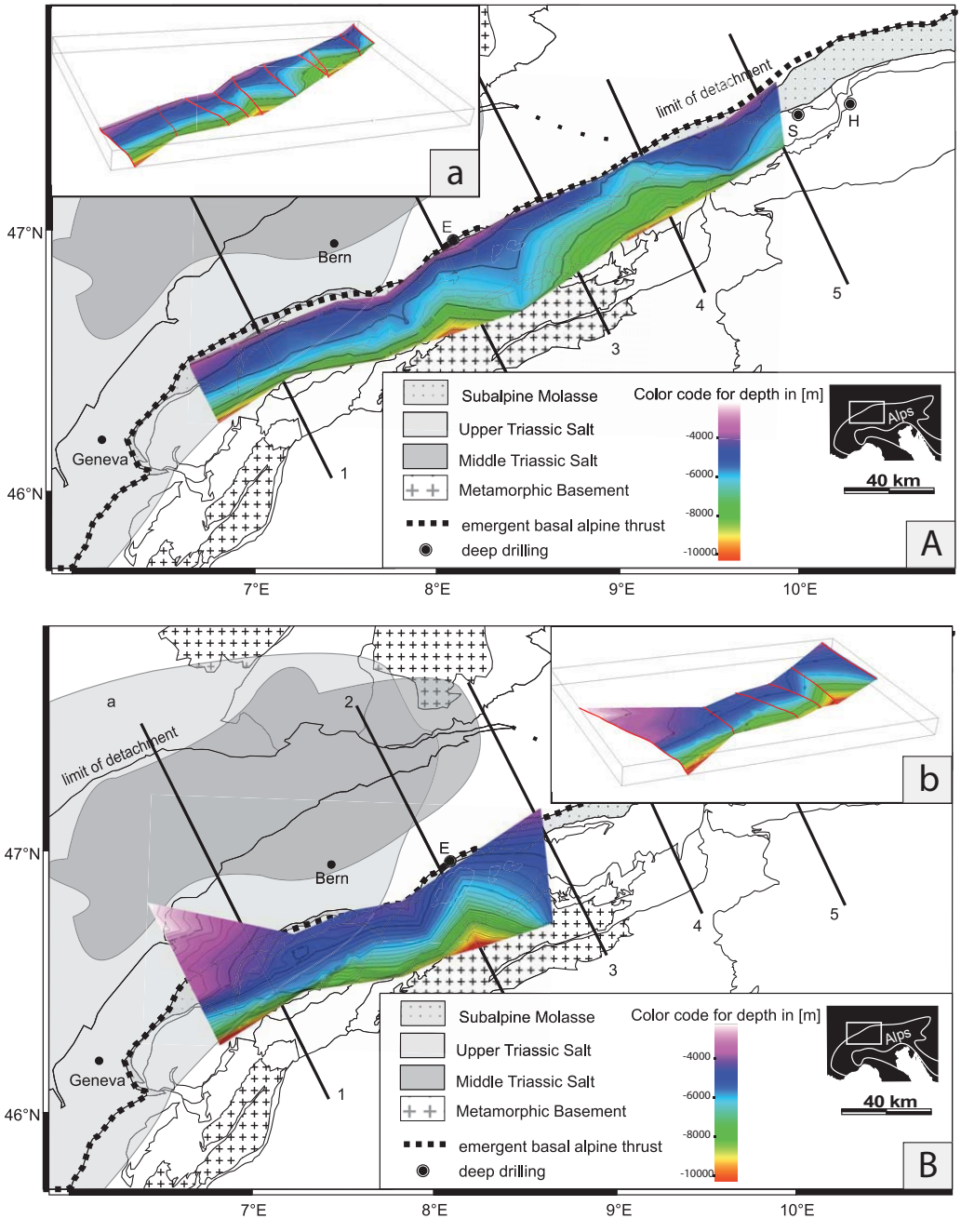

Figure 3. Construction of the basal Alpine detachment for (a) the Molasse and (b) the Jura Mountains. Detachment maps are based on available cross sections that are either balanced or interpreted from seismic lines. See insets Figures 3a and 3b for distribution of available profiles and 3-D-view of the detachment for the respective surfaces. Below the Plateau Molasse, the Jura detachment is gently dipping. Note that no F-values are calculated for the parts of the profiles south of the constructed detachment.

overburden. It is a (dimensionless) measure of horizontal to vertical stress at failure. F is analogously to W dimensionless, and a function of μ_b. F is the normalized basal shear traction at failure of the detachment [*Dahlen*, 1990; *Suppe*, 2007]. This means that F is equivalent to the sum of the effective coefficient of friction $\mu_{beff} = \mu_b^*(1-\lambda_b)$, where λ_b is the basal pore fluid pressure ratio, and normalized basal cohesion $S_b/\rho gH$. For very small F-values, basal cohesion may become an important component of the total basal shear strength. Accordingly, it is impossible to quantify the coefficient of basal friction for the wedge—F is always an upper bound for the effective basal friction—

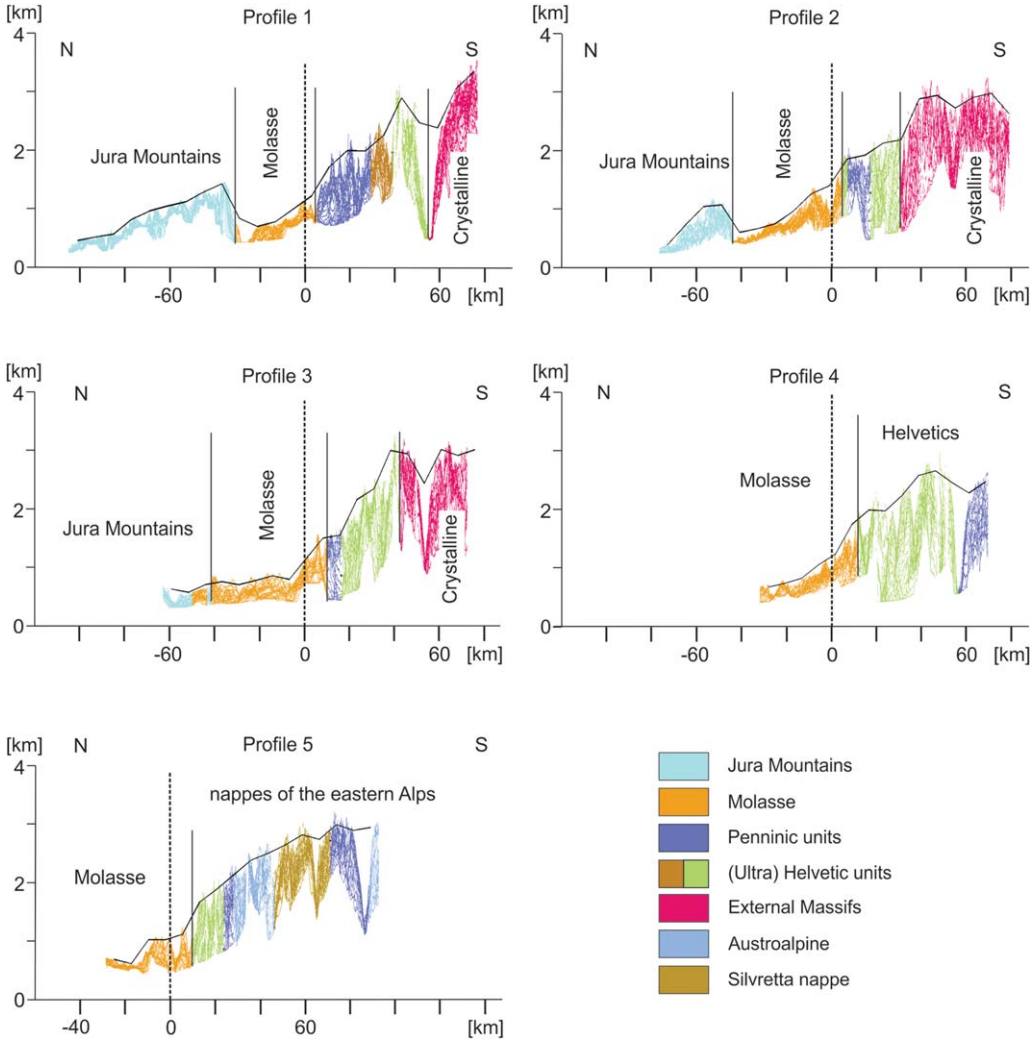

Figure 4. Swath profiles of the five cross sections. See Figure 1 for location. Colors represent different geological units of the single profiles within the swath. Origin of x axis is located at the surface break of the most external thrust of the Subalpine Molasse. Black lines show the binning results, which we used for α determination. Note the good fit, which is only slightly perturbed by major glacial valleys.

but it is possible to assess detachment and wedge strength. For details on critical taper theory, the reader is referred to *Dahlen* [1990], for the reorganization of the equation to *Suppe* [2007].

[12] Equation (3) yields all possible pairs of F and W that satisfy the critical taper theory. This allows calculating the basal detachment strength only from determination of α and β, under the assumption of the finite wedge-strength parameter W [*Suppe*, 2007].

4. The Central Alpine Critical Wedge

[13] For this analysis of the Central Alps, we use a variable, systematically determined topographic slope α and corresponding variable detachment dip β. We determined α and β along five profiles, reaching from the undeformed foreland basin to beyond the drainage divide within the orogen, thus covering the prowedge of the Central Alps (Figure 1). It is noteworthy that the results of this analysis are only valid for this part of the orogen (i.e., between the five profiles), where failure equilibrium is required. Criticality of the prowedge is independent of criticality of the retro-wedge [e.g., *Simpson*, 2011; *Graveleau et al.*, 2012]. Note that the analysis is also only valid for the present-day wedge geometry.

4.1. Construction of the Basal Detachment

[14] The basal detachment of the Alpine foreland is the Molasse detachment in the east, whereas it is

the Jura detachment in the west (Figure 3). For constructing the detachment map, we interpolated between balanced cross sections, either based on maps and reflection seismic data [*Müller*, 1984; *Menkveld*, 1995; *Burkhard and Sommaruga*, 1998; *Hänni and Pfiffner*, 2001; *Kempf and Pfiffner*, 2004; *Pfiffner*, 2010] or based on reflection seismic data only [Schmid in *Funk et al.*, 1983; *Schmid et al.*, 1996; *Pfiffner et al.*, 1997b; *Pfiffner and Hitz*, 1997; *Pfiffner et al.*, 1997c; *Pfiffner*, 2010]. For 3-D construction of the detachment, we used the GoCad software, which uses the discrete smooth interpolation algorithm [*Mallet*, 1997]. The Jura detachment below the Plateau Molasse is not shown on most available cross sections, but is gently dipping and running in the well mapped Triassic salt deposits [*Spicher*, 1980; *Philippe et al.*, 1996; *Sommaruga*, 1999]. For F-calculations, we connected the northernmost point of the Jura-detachment surface we could reconstruct from available profiles with the surface rupture of the northernmost Jura fault. This yields an upper boundary for the detachment dip and thus maximum F-values underneath the Plateau Molasse. We constructed the basal detachment to depths of maximal 10 km, which is within the seismically active zone, and thus deforming brittle (Figure 1b).

4.2. Measurement of Surface Slope

[15] We measured the corresponding α from topographic swath profiles based on the SRTM 3-arc second digital elevation model. Each swath has a width of ~15 km. We defined one representative α for segments of 7.5 km length along the profiles. We determined this value empirically. It is the best fit that represents variations in α, but smoothes out topographic effects caused by recent glacial erosion (Figure 4). To account for effects of peak uplift in response to glacial relief production [e.g., *Molnar and England*, 1990; *Montgomery*, 1994], we used the 95th percentile of the topographic data. Additionally, this value is still big enough so that local particularities will average out. We assume mechanical homogeneity for each segment.

[16] Figure 4 shows the results of the topographic analysis for the five profiles. The origin of the horizontal axis in all plots is located at the surface expression of the most external thrust within the Subalpine Molasse. Note the deeply incised Rhone Valley in Profile 1. Profiles 1 and 2 reach from the Jura Mountains in the north to the External Massifs in the south. South of the topographic step at

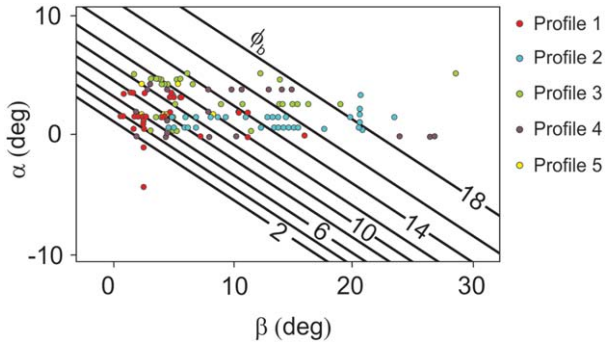

Figure 5. Alpha-beta plots for the five profiles. Diagonal lines are calculated stability field outlines for varying angles of basal friction ϕ_b (as given on the diagonal lines) (ranging from 2 to 18; $\tan\phi_b = \mu_b$), an angle of internal friction ϕ_i 30°, and hydrostatic conditions ($\lambda = 0.4$).

the southern fringe of the Jura Mountains, the topography rises quite steadily from the Molasse to the south of the Helvetic units (colored in green) and remains constant thereafter in the basement units. Note that Profile 3 still reaches the Jura Mountains in the north but the thick salt deposits in which the Jura detachment roots are not present anymore [*Philippe et al.*, 1996]. Also, the Jura detachment is absent on the adjacent cross sections. We, therefore, use the Molasse detachment for calculations. In the south of Profiles 4 and 5, Helvetic and Austroalpine nappes cover the crystalline basement. These profiles are to the east of the Jura Mountains. A similar pattern as observed in Profiles 1–3 emerges. Plotting α versus β reveals that the values do not plot on (or parallel to) any of the calculated stability fields, i.e., lines of minimum critical condition, indicating variable detachment and/or wedge strength (Figure 5).

4.3. Calculation of Strength Parameters and Assessment of Uncertainties

[17] To calculate the normalized shear strength F of the detachment with the retrieved α and their corresponding β-values according to equation (3), we use a W value of 1.0 ± 0.2, which *Suppe* [2007] determined for the European basement. Changing W within the error range affects the corresponding F-values only in the second digit and is therefore insignificant.

[18] F-values were calculated along the five investigated profiles (Figure 6). The origin of the x axis is (in analogy to Figure 4) located at the most external thrust of the Subalpine Molasse. The striking result is that a significant increase in F from north to south is required along all profiles.

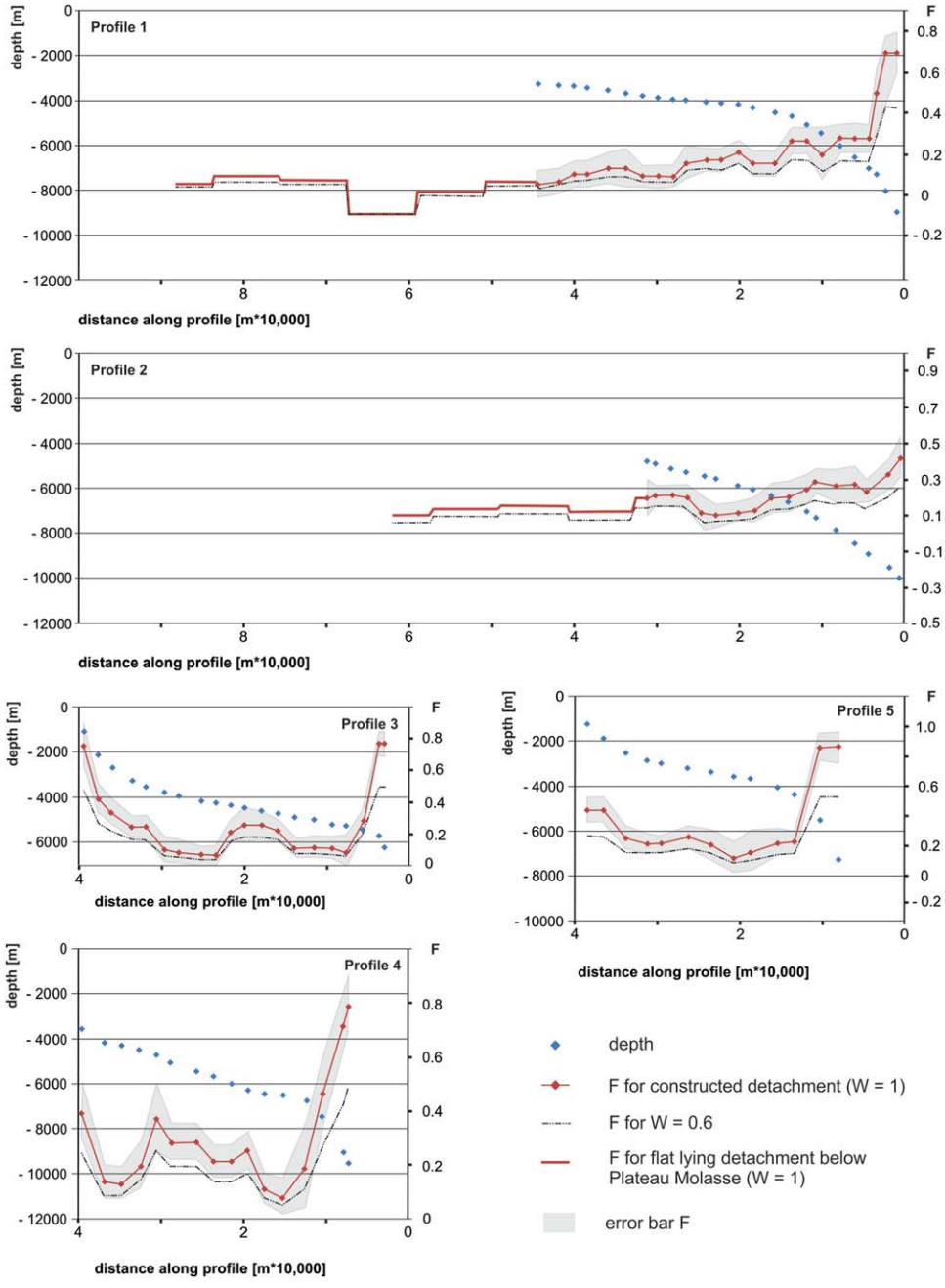

Figure 6. F-W plots of all five profiles. Origin of the *x* axis is the surface break of the most external thrust within the Subalpine Molasse. High F-values at the wedge tip (i.e., where the thrust ramps up to surface) should be read with caution, as this part is potentially not at critical state. F-values are very low in the frontal part of the wedge and increase toward the External Massifs in the south. Errors of F-values are dependent on errors within profile construction. We use a flat detachment below the Plateau Molasse for F-calculations for the Jura detachment.

In the frontal part of the wedge, F is less than 0.2. Negative F-values in Profile 1 reflect negative α-values at the southern fringe of the Jura Mountains. An increase in detachment strength occurs in all profiles south of the Subalpine Molasse, and maximum values of 0.6–0.7 are obtained to the south of the updip end of the detachment ramp underlying the Aar Massif.

[19] The uncertainty of the F-values depends on the accuracy of the profiles. Whereas the topography is easily accessible through the SRTM data,

the error of the detachment shape is difficult to quantify and generally not given in the original publications. To assess this error, we allow the detachment to vary 50 m vertically for any two points of the constructed detachment surface. The construction points on the detachment surface are irregularly spaced (due to the interpolation between the profiles) but never farther apart than 1 km, in most cases far less. In regions of high dip variations, they are only 10–50 m apart. Accordingly, 50 m of vertical variation allows β to vary at least 2.9 degrees in flat regions and more than 45 degrees elsewhere. Such variations would be visible on seismic profiles, and are accordingly overestimating the error. Consequently, uncertainty in F derived from the detachment results mostly from too high resolution in horizontal steps within the detachment, i.e., an overinterpretation of the constructed detachment surface. We, therefore, opted for a horizontal sampling distance of 2 km for the detachment that smoothes local error but still preserves the general shape of the detachment.

[20] Additional uncertainty in F is due to the scaling of lateral strength variations within the wedge. This results from spacing of weaker faults that may unload the intervening thrust sheets to below failure equilibrium [e.g., *Simpson*, 2011]. Since surface taper variations within a coherent thrust sheet may be meaningless in such a case, we chose to adopt a spatial sampling width wider than the spacing of weak faults linking surface and detachment, thereby controlling local wedge strength. A step width of 7.5 km is wider than the spacing of thrusts within the prowedge shown in maps and sections [e.g., *Müller*, 1984; *Burkhard and Sommaruga*, 1998]. The summed effect on error estimates of F of both sources of uncertainty are estimated at circa ± 0.1 (Figure 6), and still show that the result of increasing detachment strength toward the internal parts of the orogen is robust.

[21] Variations in W may occur due to lithological differences, different degrees of compaction, lithification or metamorphic overprint or different porosities, and fluid pressures. Generally, W is predicted to increase toward hinterlands through an increase in cohesion [*Fletcher*, 1989; *Dahlen*, 1990; *Suppe*, 2007; *Buiter*, 2012] and decreases at the change from brittle to ductile conditions [*Williams et al*., 1994]. In the Alps, we infer this transition on the footwall ramp approximately at a depth of 15 km (Figure 1b), based on the present-day cutoff of crustal seismicity [*Okaya et al*., 1996] and on the depth range of the 300–350°C isotherm. We calculate strength values only for areas where the detachment is brittle. In the Central Alps, it is reasonable to assume a lower W for the more external parts composed of sedimentary rocks only (as opposed to the more internal crystalline massifs). The sedimentary western Taiwan wedge has a value of $W = 0.6$ [*Suppe*, 2007]—a value also found in wells drilling sedimentary sequences [*Zoback and Townend*, 2001]. Recalculating F with $W = 0.6$, leads to a general reduction in detachment strength (and an even more pronounced difference of F-values from north to south) (Figure 6). Hence, the values in Figure 6 are maximum estimates. However, the difference between the calculations for the part of the wedge that consists of sediments is negligible.

5. Correlation of Wedge Mechanics And Observed Geology

[22] Inferred F-values correlate with the lithology of the detachment, as can be observed on a detachment strength map (Figure 7). As expected from previous studies [e.g., *Philippe*, 1994; *Letouzey et al*., 1995; *Sommaruga*, 1999], the friction values are lowest (<0.05) below the Jura Mountains and the western Plateau Molasse, where the detachment is running in Triassic evaporites. These salt deposits pinch out toward east and south [*Philippe*, 1994; *Sommaruga*, 1999], and are lacking in the central part of the study area (Figure 7). Intercalations of anhydrite and shales are reported from the Entlebuch deep drilling at the detachment depth [*Vollmayr and Wendt*, 1987]. These shale-sulfate multilayers may also become very weak [*Jordan and Nüesch*, 1989]. The southward continuation of this interlayering is not fully known, but the Triassic sequence in the hangingwall cover of the Aar Massif does not show evaporite remnants apart from some cargneule with a thickness of less than 2 m [*Krayenbuhl and Steck*, 2009]. This suggests a south to south-eastward disappearance of evaporites and a predominance of shales, marls, and limestones at the detachment level. The Triassic sequences further to the southwest (external Massifs in the French Alps) contain more abundant remnants of cargneule and evaporites. Note that F-values calculated for evaporites may not be interpreted as μ_b in a mechanical sense, as at the detachment depth halite and anhydrite already show ductile behavior. The value is hence an apparent friction, equivalent to the shear resistance of the

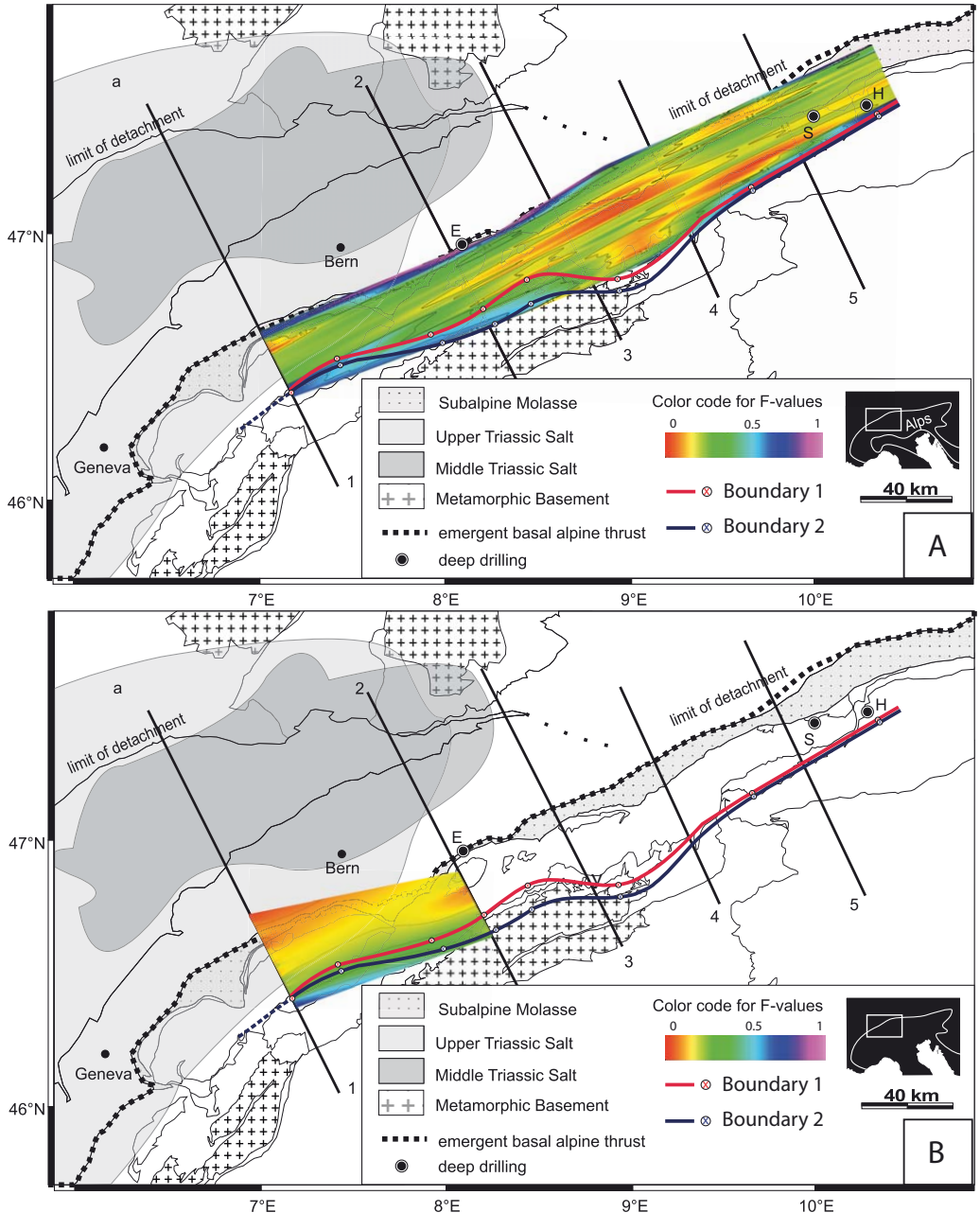

Figure 7. Detachment strength (F-value) map and its correlation with geology. Red line denotes the hangingwall cutoff of crystalline basement overthrust on sediments, black line denotes footwall cutoff of basement from where on the detachment runs through crystalline rocks only. Where the detachment is running through the salt deposits, the strength is lowest (<0.1), as is known from previous studies. The rapid increase in detachment strength (F-values respectively) coincides with this change in detachment lithology. E, S, and H are the Entlebuch, Sulzberg, and Hindelang deep drillings; a denotes autochthonous Jura, f denotes folded Jura. Note the rapid increase in F-values at the front of the External Crystalline Massifs. Limit of the detachment taken from *Spicher* [1980] and *Schmid et al*. [2004]. The transition of the detachment limit between the Jura Mountains and the eastern Subalpine Molasse is only poorly constrained and possibly a complex zone (dotted line). Salt distribution is taken from *Philippe et al*. [1996]. North of boundary 1, the detachment runs in sedimentary rocks and the overlying wedge consists of sedimentary rocks, between boundary 1 and boundary 2, crystalline rocks are thrust over sedimentary rocks, south of boundary 2 the detachment runs in crystalline rocks. Constraint points are from profiles used for detachment construction.

evaporites. From *Dahlen*'s [1990] assessment of these equations to evaporites, this remaining strength may be largely equivalent to the normalized cohesion of viscous rocks (see above).

[23] In the eastern part of the study area, where the basal detachment is localized stratigraphically between Upper Cretaceous/Tertiary pelites in the footwall and Triassic marls in the hangingwall [e.g., *Bachmann and Müller*, 1981; *Auer and Eisbacher*, 2003; *Berge and Veal*, 2005], the values are comparably low (~ 0.1). Very low F-values are also reported from the Makran and the Nankai wedge [*Schott and Koyi*, 2001] and from Taiwan [*Suppe*, 2007]. They are much lower than effective friction coefficients measured on shales in laboratories [e.g., *Byerlee*, 1978; *Kopf and Brown*, 2003; *den Hartog et al*., 2012; *Saffer et al*., 2012]. This is generally attributed to high pore fluid pressures. *Suppe* [2007] notes that no excess pore pressure was found in a well drilling the Taiwan detachment. In the eastern part of the Central Alps, slightly elevated pore fluid pressures are reported from the deep drillings Sulzberg-1 and Hindelang-1 [*Müller et al*., 1988]. The Sulzberg-1 drilling reaches the basement and penetrates the basal detachment at a depth of 4280 m, after drilling through Molasse sediments [*Herrmann et al*., 1985]. At detachment depth, the pore fluid pressure is ~57 MPa [*Müller et al*., 1988] rising from a near hydrostatic pressure gradient in the hangingwall to an elevated gradient of 0.2–0.4 MPa/10 m approaching the detachment. Using typical values for the density of the Molasse sediments of 2.5 g/cm^3 [e.g., *Schärli*, 1989], the corresponding lithostatic pressure is 107 MPa. This results in a λ-value of 0.53, which is only slightly higher than hydrostatic (~0.4), and less than lithostatic. The drilling Hindelang-1 does not reach the basement or the basal detachment but includes the Helvetic detachment—the detachment formed prior to the current Alpine detachment. The pore fluid pressure rises toward this level and reaches ~74 MPa [*Müller et al*., 1988]. Using typical density values for limestone of 2.7 g/cm^3 dominating the hangingwall, the corresponding lithostatic pressure is 137.5 MPa, and λ is 0.53. However, it has also been noted that precise determination of pore pressure in shales with well-logging tools may be affected by extremely low permeability—typically leading to an underestimate of true pressures [e.g., *Chang et al*., 2006]. Hence, elevated pore pressures in shale-dominated lithologies presumably are below the true values. They may contribute but may also be insufficient to explain the very low values of detachment strength. Using a basal friction coefficient μ_b of 0.7 for shale-dominated shear zones [*den Hartog et al*., 2012], a μ_{beff} of 0.2 requires a λ_b of 0.7 (from $\mu_{beff} = \mu_b^*(1-\lambda_b)$, see above). For strength values of 0.05 in shales, λ_b should be 0.93 which is almost lithostatic pore fluid pressure. Therefore, either excess pore pressures is a transient feature during seismic rupture or a rapid creep event or other ill-defined aspects related to weakening in shales play a key role.

6. Implications for Alpine Evolution and Comparison to Other Orogens

[24] The weak shale detachment of the Subalpine Molasse is interesting in the light of the Neogene shortening history of the Alps. Shortening in the Jura Mountains commenced at ~10 Ma [*Bollinger et al*., 1993]. Generally, this is considered to coincide with the termination of thrusting within the Subalpine Molasse. Recently, however, it was discovered that approximately two thirds of total shortening within the Subalpine Molasse occurred while the Jura Mountains formed [*von Hagke et al*., 2012]. The minor difference in detachment strength between the salt and shale detachments may help to explain why shortening did not entirely shift into the Jura Mountains but also continued in the Subalpine Molasse despite the evaporites entering the wedge. Thus, the role of salt as the major detaching horizon for the Neogene shortening history of the Alps may be overrated, most probably because of the prominent external position and geomorphic expression of the Jura fold and thrust belt. Finally, initiation of the Molasse detachment is reported to be at around 24–20 Ma [*Schlunegger et al*., 1997; *Kempf et al*., 1999], based on magnetostratigraphic constraints. After this period, internal shortening within the Alpine wedge rapidly terminated and deformation was shifted to the orogenic front in the north [see compilation by *Schmid et al*., 1996], as well as into the Orobic Alps in the Alpine retro-wedge to the south. We, therefore, speculate that initiation of this shale-dominated detachment, and its maturation into a very weak fault has led to focusing subsequent shortening on the northern flank of the Alps into the Subalpine Molasse.

[25] *Handy et al*. [2010] calculate a convergence rate of ~2 mm/a since 19 Ma [*Capitanio and Goes*, 2006]. Recent re-evaluation of the shortening rate of the Central Alpine prowedge above the Molasse detachment based on reconstruction of its

exhumation history in thrust hangingwalls [*von Hagke et al*., 2012] yields ~1.2 mm/a since 10 Ma, indicating that since at least that time some 60% of the above convergence is localized in the Subalpine Molasse (the remaining 40% are focused in coeval deformation of the Southern Alps and the Jura Mountains [e.g., *Schönborn*, 1992; *Burkhard and Sommaruga*, 1998]). Hence, activation of the Molasse detachment appears to have been instrumental for the partitioning of Central Alpine deformation in the terminal stage of their evolution.

[26] The importance of transient weakening of shale detachments underlying thin-skinned fold and thrust belts and the fundamental role for orogenic evolution is becoming increasingly recognized. In addition to Taiwan [*Suppe*, 2007], equally low transient friction values have been reported from the Himalayas [e.g., *Avouac*, 2008; *Herman et al*., 2010], and the Andean foreland belt [*Oncken et al*., 2012]. In addition to permanent fluid overpressures at the detachment, frictional melting, hydrodynamic lubrication, or thermal fluid pressurization may be held responsible for weakening the shale detachments during rupture and slip [*Kanamori and Brodsky*, 2004], supporting progressive localization of orogenic deformation into such systems.

7. Summary and Conclusions

[27] This study extends the wedge mechanical approach of *Suppe* [2007] and revealed variations in strength of the Central Alpine basal detachment. We propose a way to obtain representative surface-slope values for critical wedge analysis, for which so far no standardized method is used. This theoretical approach is applicable in the Central Alps. The results show that the effective basal friction coefficient in the frontal part of the wedge is extremely low (<0.2 in shale-dominated sediment, and <0.1 within evaporites). Fluids appear to be only mildly overpressured in well logs, insufficient to explain the very low strength values. In contrast, a comparatively high detachment strength between 0.4 and 0.7 was obtained for the crystalline hinterland, suggesting no relevant fluid overpressuring in basement rocks. These changes in detachment strength coincide with changes of detachment lithology in the hangingwall and footwall, respectively, emphasizing the dominant role of weak shales. Finally, evolution of a weak shale-dominated detachment may have been responsible for localizing late deformation of the prowedge of the Central Alps into the Subalpine Molasse.

Acknowledgments

[28] Nadaya Cubas and Olaf Zielke helped with Matlab coding. This manuscript benefited from discussions with Oliver Heidbach, Friedhelm von Blanckenburg, Tibi Codilean, Mark Handy, Kamil Ustaszewski, and Fang-Lin Wang. This research was conducted in the framework of the ESF TopoEurope CRP "Thermo-Europe." The German Research Foundation (DFG) provided funding by research grant number CE 175/1-1. John Suppe, Jon Mosar, Jean-Pierre Burg, and one anonymous reviewer are thanked for constructive reviews; Joel Baker and Janne Blichert-Toft are thanked for editorial handling.

References

Auer, M., and G. H. Eisbacher (2003), Deep structure and kinematics of the Northern Calcareous Alps (TRANSALP Profile), *Int. J. Earth Sci.*, *92*(2), 210–227.

Avouac, J. P. (2008), Dynamic processes in extensional and compressional settings—Mountain building: From earthquakes to geological deformation, *Treatise Geophys.*, *6*, 377–439.

Baby, P., B. Colletta, and D. Zubieta (1995), Etude géométrique et expérimentale d'un bassin transporté: Exemple du synclinorium de l'Alto Beni (Andes centrales), *Bull. Soc. Géol. Fr.*, *166*(6), 797–811.

Bachmann, C. E., S. Wiemer, J. Woessner, and S. Hainzl (2011), Statistical analysis of the induced Basel 2006 earthquake sequence: Introducing a probability-based monitoring approach for Enhanced Geothermal Systems, *Geophys. J.*, *186*(2), 793–807.

Bachmann, G. H., and M. Müller (1981), Tiefbohrung Vorderriß 1, (Kalkalpen, Bayern), *Geol. Bavarica*, *81*, 17–53.

Berge, T. B., and S. L. Veal (2005), Structure of the Alpine foreland, *Tectonics*, *24*, TC5011, doi:10.1029/2003TC001588.

Berger, J. P., B. Reichenbacher, D. Becker, M. Grimm, K. Grimm, L. Picot, A. Storni, C. Pirkenseer, and A. Schaefer (2005), Eocene-Pliocene time scale and stratigraphy of the Upper Rhine Graben (URG) and the Swiss Molasse Basin (SMB), *Int. J. Earth Sci.*, *94*(4), 711–731.

Bianchetti, G., P. Roth, and F.-D. Vuataz (1992), Deep groundwater circulation in the Alps: Relations between water infiltration, induced seismicity and thermal springs: The case of Val d'Illiez, Wallis, Switzerland, *Eclogae Geol. Helv.*, *85*(2), 291–305.

Bollinger, T., B. Engesser, and M. Weidmann (1993), Première découverte de mammifères pliocènes dans le Jura neuchâtelois, *Eclogae Geol. Helv.*, *86*(3), 1031–1068.

Bose, S., N. Mandal, D. K. Mukhopadhyay, and P. Mishra (2009), An unstable kinematic state of the Himalayan tectonic wedge: Evidence from experimental thrust-spacing patterns, *J. Struct. Geol.*, *31*(1), 83–91.

Boyer, S. E., and D. Elliott (1982), Thrust systems, *AAPG Bull.*, *66*(9), 1196–1230.

Buiter, S. J. H. (2012), A review of brittle compressional wedge models, *Tectonophysics*, *530–531*, 1–17.

Burkhard, M. (1990), Aspects of large-scale Miocene deformation in the most external part of the Swiss Alps (Subalpine Molasse to Jura fold belt), *Eclogae Geol. Helv.*, *83*(3), 559–583.

Burkhard, M., and A. Sommaruga (1998), Evolution of the western Swiss Molasse basin: Structural relations with the Alps and the Jura belt, *Geol. Soc. Spec. Publ.*, *134*, 279–298.

Buxtorf, A. (1907), Zur Tektonik des Kettenjura, *Ber. Versammlungen oberrheinischen Geol. Vereins*, *40*, 29–38.

Buxtorf, A. (1916), Prognosen und Befunde beim Hauensteinbasis-und Grenchenbergtunnel und die Bedeutung der letzteren für die Geologie des Juragebirges, *Verh. Naturforsch. Ges. Basel*, *27*, 184–205.

Byerlee, J. (1978), Friction of rocks, *Pure Appl. Geophys.*, *116*(4), 615–626.

Calais, E., J.-M. Nocquet, F. Jouanne, and M. Tardy (2002), Current strain regime in the Western Alps from continuous Global Positioning System measurements, 1996–2001, *Geology*, *30*(7), 651–654.

Calassou, S., C. Larroque, and J. Malavieille (1993), Transfer zones of deformation in thrust wedges: An experimental study, *Tectonophysics*, *221*(3–4), 325–344.

Capitanio, F. A., and S. Goes (2006), Mesozoic spreading kinematics: Consequences for Cenozoic Central and Western Mediterranean subduction, *Geophys. J.*, *165*(3), 804–816.

Chang, C., M. D. Zoback, and A. Khaksar (2006), Empirical relations between rock strength and physical properties in sedimentary rocks, *J. Petrol. Sci. Eng.*, *51*(3–4), 223–237.

Couzens-Schultz, B. A., B. C. Vendeville, and D. V. Wiltschko (2003), Duplex style and triangle zone formation: Insights from physical modeling, *J. Struct. Geol.*, *25*(10), 1623–1644.

Cubas, N., J. P. Avouac, Y. M. Leroy, and A. Pons (2013), Low friction along the high slip patch of the 2011 Mw 9.0 Tohoku-Oki earthquake required from the wedge structure and extensional splay faults, *Geophys. Res. Lett.*, *40*, 4231–4237, doi:10.1002/grl.50682.

Dahlen, F. A. (1984), Noncohesive critical coulomb wedges: An exact solution, *J. Geophys. Res.*, *89*(B12), 10,125–10,133.

Dahlen, F. A. (1990), Critical taper model of fold-and-thrust belts and accretionary wedges, *Annu. Rev. Earth Planet. Sci.*, *18*, 55–99.

Dahlen, F. A., J. Suppe, and D. Davis (1984), Mechanics of fold-and-thrust belts and accretionary wedges: Cohesive coulomb theory, *J. Geophys. Res.*, *89*(B12), 10,087–10,101.

Davis, D., and R. von Huene (1987), Inferences on sediment strength and fault friction from structures at the Aleutian Trench, *Geology*, *15*(6), 517–522.

Davis, D., J. Suppe, and F. A. Dahlen (1983), Mechanics of fold-and-thrust belts and accretionary wedges, *J. Geophys. Res.*, *88*(B2), 1153–1172.

Deichmann, N. (2010), *Earthquakes in Switzerland and Surrounding Regions 1996–2009 Version 2010.1*, Swiss Seismol. Serv—ETH Zürich, Zurich, Switzerland.

Deichmann, N., and J. Ernst (2009), Earthquake focal mechanisms of the induced seismicity in 2006 and 2007 below Basel (Switzerland), *Swiss J. Geosci.*, *102*(3), 457–466.

Deichmann, N., and I. Marschall (2002), *Focal Mechanism Catalog of Earthquakes in Switzerland and Neighboring Countries, Compiled for Project PEGASOS*, Swiss Seismol. Serv.—ETH Zürich, Zurich, Switzerland.

Deichmann, N., M. Baer, J. Braunmiller, S. Husen, D. Fäh, D. Giardini, P. Kästli, U. Kradolfer, and S. Wiemer (2006), Earthquakes in Switzerland and surrounding regions during 2005, *Eclogae Geol. Helv.*, *99*(3), 443–452.

den Hartog, S. A. M., A. R. Niemeijer, and C. J. Spiers (2012), New constraints on megathrust slip stability under subduction zone P–T conditions, *Earth Planet. Sci. Lett.*, *353–354*, 240–252.

Escher, A., and C. Beaumont (1997), Formation, burial and exhumation of basement nappes at crustal scale: A geometric model based on the Western Swiss-Italian Alps, *J. Struct. Geol.*, *19*(7), 955–974.

Fäh, D., et al. (2011), *ECOS-09 Earthquake Catalogue of Switzerland Release 2011. Report and Database*, Swiss Seismol. Serv. ETH Zürich, Zurich, Switzerland.

Fäh, D., et al. (2012), Coupled seismogenic geohazards in Alpine regions, *Bollettino Geofis. Teor. Appl.*, *53*(4), 485–508.

Fletcher, R. C. (1989), Approximate analytical solutions for a cohesive fold-and-thrust wedge: Some results for lateral variation of wedge properties and for finite wedge angle, *J. Geophys. Res.*, *94*(B8), 10,347–10,354.

Frisch, W. (1979), Tectonic progradation and plate tectonic evolution of the Alps, *Tectonophysics*, *60*(3–4), 121–139.

Fügenschuh, B., and S. M. Schmid (2003), Late stages of deformation and exhumation of an orogen constrained by fission-track data: A case study in the Western Alps, *Geol. Soc. Am. Bull.*, *115*(11), 1425–1440.

Funk, H., T. Labhart, A. G. Milnes, O. A. Pfiffner, U. Schaltegger, C. Schindler, S. M. Schmid, and R. Trümpy (1983), Bericht über die Jubiläumsexkursion «Mechanismus der Gebirgsbildung» der Schweizerischen Geologischen Gesellschaft in das ost-und zentralschweizerische Helvetikum und in das nördliche Aarmassiv vom 12. bis 17. September 1982, *Eclogae Geol. Helv.*, *76*(1), 91–123.

Gebauer, D. (1999), Alpine geochronology of the Central and Western Alps: New constraints for a complex geodynamic evolution, *Schweiz. Mineral. Petrogr. Mitt.*, *79*, 191–208.

Giamboni, M., K. Ustaszewski, S. M. Schmid, M. E. Schumacher, and A. Wetzel (2004), Plio-Pleistocene transpressional reactivation of Paleozoic and Paleogene structures in the Rhine-Bresse transform zone (northern Switzerland and eastern France), *Int. J. Earth Sci.*, *93*(2), 207–223.

Graveleau, F., J. Malavieille, and S. Dominguez (2012), Experimental modelling of orogenic wedges: A review, *Tectonophysics*, *538–540*, 1–66.

Gupta, H. K., B. K. Rastogi, and H. Narain (1972), Common features of the reservoir-associated seismic activities, *Bull. Seismol. Soc. Am.*, *62*(2), 481–492.

Handy, M. R., S. M. Schmid, R. Bousquet, E. Kissling, and D. Bernoulli (2010), Reconciling plate-tectonic reconstructions of Alpine Tethys with the geological-geophysical record of spreading and subduction in the Alps, *Earth Sci. Rev.*, *102*(3–4), 121–158.

Hänni, R., and O. A. Pfiffner (2001), Evolution and internal structure of the Helvetic nappes in the Bernese Oberland, *Eclogae Geol. Helv.*, *94*, 161–171.

Häring, M. O., U. Schanz, F. Ladner, and B. C. Dyer (2008), Characterisation of the Basel 1 enhanced geothermal system, *Geothermics*, *37*(5), 469–495.

Heidbach, O., and J. Reinecker (2012), Analyse des rezenten Spannungsfeldes der Nordschweiz, *Nagra Arbeitsbericht*, *2012-05*, 84 S.

Heidbach, O., M. Tingay, A. Barth, J. Reinecker, D. Kurfeß, and B. Müller (2008), *The 2008 Release of the World Stress Map*, GFZ Potsdam, Potsdam, Germany., [Available at www.world-stress-map.org.]

Herman, F., et al. (2010), Exhumation, crustal deformation, and thermal structure of the Nepal Himalaya derived from the inversion of thermochronological and thermobarometric data and modeling of the topography, *J. Geophys. Res.*, *115*, B06407, doi:10.1029/2008JB006126.

Herrmann, P., I. Draxler, and M. Müller (1985), *Erläuterungen zu Blatt 83 Sulzberg*, 20 p., Geol. Bundesanst., Wien.

Homewood, P. W., P. A. Allen, and G. D. Williams (1986), Dynamics of the Molasse Basin of western Switzerland, in *Foreland Basins*, edited by P. A. Allen and P. W. Homewood, pp. 199–217, Int. Assoc. of Sedimentol., Oxford, U. K.

Husen, S., C. E. Bachmann, and D. Giardini (2007), Locally triggered seismicity in the central Swiss Alps following the large rainfall event of August 2005, *Geophys. J.*, *171*(3), 1126–1134.

Husen, S., E. Kissling, and A. von Deschwanden (2012), Induced seismicity during the construction of the Gotthard Base Tunnel, Switzerland: Hypocenter locations and source dimensions, *J. Seismol.*, *16*(2), 1–19.

Jordan, P., and R. Nüesch (1989), Deformational behavior of shale interlayers in evaporite detachment horizons, jura overthrust, Switzerland, *J. Struct. Geol.*, *11*(7), 859–871.

Kanamori, H., and E. E. Brodsky (2004), The physics of earthquakes, *Rep. Prog. Phys.*, *67*(8), 1429.

Kastrup, U., M. L. Zoback, N. Deichmann, K. F. Evans, D. Giardini, and A. J. Michael (2004), Stress field variations in the Swiss Alps and the northern Alpine foreland derived from inversion of fault plane solutions, *J. Geophys. Res.*, *109*, B01402, doi:10.1029/2003JB002550.

Kempf, O., and O. A. Pfiffner (2004), Early tertiary evolution of the North Alpine Foreland Basin of the Swiss Alps and adjoining areas, *Basin Res.*, *16*(4), 549–567.

Kempf, O., A. Matter, D. W. Burbank, and M. Mange (1999), Depositional and structural evolution of a foreland basin margin in a magnetostratigraphic framework: The eastern Swiss Molasse, *Int. J. Earth Sci.*, *88*(2), 253–275.

Kopf, A., and K. M. Brown (2003), Friction experiments on saturated sediments and their implications for the stress state of the Nankai and Barbados subduction thrusts, *Mar. Geol.*, *202*(3–4), 193–210.

Krayenbuhl, T., and A. Steck (2009), Structure and kinematics of the Jungfrau syncline, Faflertal (Valais, Alps), and its regional significance, *Swiss J. Geosci.*, *102*(3), 441–456.

Lacombe, O., and F. Mouthereau (2002), Basement-involved shortening and deep detachment tectonics in forelands of orogens: Insights from recent collision belts (Taiwan, Western Alps, Pyrenees), *Tectonics*, *21*(4), 1030, doi:10.1029/2001TC901018.

Lammerer, B., H. Gebrande, E. Lüschen, and P. Veselá (2008), A crustal-scale cross-section through the Tauern Window (eastern Alps) from geophysical and geological data, *Geol. Soc. Spec. Publ.*, *298*(1), 219–229.

Laubscher, H. (1961), Die Fernschubhypothese der Jurafaltung, *Eclogae Geol. Helv.*, *54*(1), 221–282.

Laubscher, H. (1977), Fold development in the Jura, *Tectonophysics*, *37*(4), 337–362.

Laubscher, H. (1986), The eastern Jura: Relations between thin-skinned and basement tectonics, local and regional, *Geol. Rundsch.*, *75*(3), 535–553.

Letouzey, J., B. Colletta, R. Vially, and J. C. Chermette (1995), Evolution of salt-related structures in compressional settings, in *Salt Tectonics: A Global Perspective, Am. Assoc. Pet. Geol. Mem. 65*, edited by M. P. A. Jackson, D. G. Roberts, and S. Snelson, pp. 41–60., American Association of Petroleum Geologists, Tulsa, OK, USA.

Liu, C. C., A. T. Linde, and I. S. Sacks (2009), Slow earthquakes triggered by typhoons, *Nature*, *459*(7248), 833–836.

Lohrmann, J., N. Kukowski, J. Adam, and O. Oncken (2003), The impact of analogue material properties on the geometry, kinematics, and dynamics of convergent sand wedges, *J. Struct. Geol.*, *25*(10), 1691–1711.

Lüschen, E., D. Borrini, H. Gebrande, B. Lammerer, K. Millahn, F. Neubauer, and R. Nicolich (2006), TRANSALP–deep crustal Vibroseis and explosive seismic profiling in the Eastern Alps, *Tectonophysics*, *414*(1–4), 9–38.

Macedo, J. M. B., L. M. F. Gottschalk, and E. P. S. Bon (1999), Calcium carbonate mediates higher lignin peroxidase activity in the culture supernatant of Streptomyces Viridosporus T7A, *Braz. J. Chem. Eng.*, *16*, 163–169.

Madritsch, H., S. M. Schmid, and O. Fabbri (2008), Interactions between thin- and thick-skinned tectonics at the northwestern front of the Jura fold-and-thrust belt (Eastern France), *Tectonics*, *27*, TC5005, doi:10.1029/2008TC002282.

Madritsch, H., F. Preusser, O. Fabbri, V. Bichet, F. Schlunegger, and S. M. Schmid (2010), Late quaternary folding in the Jura Mountains: Evidence from syn-erosional deformation of fluvial meanders, *Terra Nova*, *22*(2), 147–154.

Mallet, J. (1997), Discrete modeling for natural objects, *Math. Geol.*, *29*(2), 199–219.

Mandal, N., A. Chattopadhyay, and S. Bose (1997), Imbricate thrust spacing: Experimental and theoretical analyses, in *Evolution of Geological Structures in Micro to Macroscales*, edited by S. Sengupta, pp. 143–165, Chapman and Hall, London.

Menkveld, J.-W. (1995), *Der geologische Bau des Helvetikums der Innerschweiz*, PhD thesis, 165 pp., Univ. Bern, Bern.

Molnar, P., and P. England (1990), Late Cenozoic uplift of mountain ranges and global climate change: Chicken or egg?, *Nature*, *346*(6279), 29–34.

Montgomery, D. R. (1994), Valley incision and the uplift of mountain peaks, *J. Geophys. Res.*, *99*(B7), 13,913–13,921.

Mosar, J. (1999), Present-day and future tectonic underplating in the western Swiss Alps: Reconciliation of basement/wrench-faulting and decollement folding of the Jura and Molasse basin in the Alpine foreland, *Earth Planet. Sci. Lett.*, *173*(3), 143–155.

Müller, M. (1984), Bau, Untergrund und Herkunft der Allgäuer Faltenmolasse: Mit 4 Abbildungen, *Jahresberichte Mitt. Oberrheinischen Geol. Ver., Neue Folge*, *66*, 321–328.

Müller, M., F. Nieberding, and A. Wanninger (1988), Tectonic style and pressure distribution at the northern margin of the Alps between Lake Constance and the River Inn, *Geol. Rundsch.*, *77*(3), 787–796.

Okaya, N., S. Cloetingh, and S. Mueller (1996), A lithospheric cross-section through the Swiss Alps—II. Constraints on the mechanical structure of a continent-continent collision zone, *Geophys. J.*, *127*(2), 399–414.

Oncken, O., D. Boutelier, G. Dresen, and K. Schemmann (2012), Strain accumulation controls failure of a plate boundary zone: Linking deformation of the Central Andes and lithosphere mechanics, *Geochem. Geophys. Geosyst.*, *13*, Q12007, doi:10.1029/2012GC004280.

Persaud, M., and O. A. Pfiffner (2004), Active deformation in the eastern Swiss Alps: Post-glacial faults, seismicity and surface uplift, *Tectonophysics*, *385*(1–4), 59–84.

Pfiffner, O. A. (1986), Evolution of the north Alpine foreland basin in the Central Alps, in *Foreland Basins*, edited by P. A. Allen and P. W. Homewood, pp. 219–228, Int. Assoc. of Sedimentol., Oxford, U. K.

Pfiffner, O. A. (2010), *Geologie der Alpen*, 2 erweiterte Auflage ed., 360 pp., Uni Taschenbuecher (UTB)/Haupt Verlag, Bern.

Pfiffner, O. A., and L. Hitz (1997), Geologic interpretation of the seismic profiles of the eastern Traverse (lines E1-E3,

E7-E9): Eastern Swiss Alps, in *Deep Structure of the Swiss Alps: Results of NRP 20*, edited by O. A. Pfiffner et al., pp. 73–100, Birkhäuser, Basel, Switzerland.

Pfiffner, O. A., W. Frei, P. Valasek, M. Stäuble, L. Levato, L. DuBois, S. M. Schmid, and S. B. Smithson (1990), Crustal shortening in the Alpine Orogen: Results from deep seismic reflection profiling in the eastern Swiss Alps, Line NFP 20-east, *Tectonics*, *9*(6), 1327–1355.

Pfiffner, O. A., S. Sahli, and M. Stäuble (1997a), Compression and uplift of the external massifs in the Helvetic zone, in *Deep Structure of the Swiss Alps: Results of NRP 20*, edited by O. A. Pfiffner et al., pp. 139–153, Birkhäuser, Basel, Switzerland.

Pfiffner, O. A., P.-F. Erard, and M. Stäuble (1997b), Two cross sections through the Swiss Molasse basin (lines E4-E6, W1, W7-W110), in *Deep Structure of the Swiss Alps: Results of NRP 20*, edited by O. A. Pfiffner et al., pp. 64–72, Birkhäuser, Basel, Switzerland.

Pfiffner, O. A., P. Lehner, P. Heitzmann, S. Müller, and A. Steck (1997c), *Deep Structure of the Swiss Alps. Results of NRP 20*, Birkhäuser, Basel, Switzerland.

Philippe, Y. (1994), Transfer zone in the Southern Jura thrust belt (Eastern France): Geometry, development, and comparison with analogue modeling experiments, *Hydrocarbon and Petroleum Geology in France, Spec. Publ. Eur. Assoc. Pet. Geosci. 4*, pp. 327–346, Springer Verlag, Berlin, Heidelberg.

Philippe, Y., B. Colletta, E. Deville, and A. Mascle (1996), The Jura fold-and-thrust belt: A kinematic model based on map-balancing, in *Peri-Tethys Memoir 2: Structure and Prospects of Alpine Basins and Forelands*, edited by P. A. Ziegler and F. Horvath, pp. 235–261, Ed. du Mus. Natl. d'Histoire Nat., Paris.

Ripperger, J., P. Kästli, D. Fäh, and D. Giardini (2009), Ground motion and macroseismic intensities of a seismic event related to geothermal reservoir stimulation below the city of Basel—Observations and modelling, *Geophys. J.*, *179*(3), 1757–1771.

Roth, P., N. Pavoni, and N. Deichmann (1992), Seismotectonics of the eastern Swiss Alps and evidence for precipitation-induced variations of seismic activity, *Tectonophysics*, *207*(1–2), 183–197.

Rothé, J. P. (1970), Seismes artificiels, *Tectonophysics*, *9*(2–3), 215–238.

Ruh, J. B., B. J. P. Kaus, and J.-P. Burg (2012), Numerical investigation of deformation mechanics in fold-and-thrust belts: Influence of rheology of single and multiple décollements, *Tectonics*, *31*, TC3005, doi:10.1029/2011TC003047.

Saffer, D. M., D. A. Lockner, and A. McKiernan (2012), Effects of smectite to illite transformation on the frictional strength and sliding stability of intact marine mudstones, *Geophys. Res. Lett.*, *39*, L11304, doi:10.1029/2012GL051761.

Schärli, U. (1989), Geothermische Detailkartierung (1: 100000) in der zentralen Nordschweiz mit besonderer Berücksichtigung petrophysikalischer Parameter, PhD thesis, 166 pp., ETH Zurich, Zurich, Switzerland.

Schlunegger, F., A. Matter, D. W. Burbank, and E. M. Klaper (1997), Magnetostratigraphic constraints on relationships between evolution of the central Swiss Molasse basin and Alpine orogenic events, *Geol. Soc. Am. Bull.*, *109*(2), 225–241.

Schmid, S. M., and E. Kissling (2000), The arc of the western Alps in the light of geophysical data on deep crustal structure, *Tectonics*, *19*(1), 62–85.

Schmid, S. M., O. A. Pfiffner, N. Froitzheim, G. Schönborn, and E. Kissling (1996), Geophysical-geological transect and tectonic evolution of the Swiss-Italian Alps, *Tectonics*, *15*(5), 1036–1064.

Schmid, S. M., B. Fügenschuh, E. Kissling, and R. Schuster (2004), Tectonic map and overall architecture of the Alpine orogen, *Eclogae Geol. Helv.*, *97*(1), 93–117.

Schönborn, G. (1992), Alpine tectonics and kinematic models of the central Southern Alps, *Mem. Sci. Geol.*, *44*, 229–393.

Schott, B., and H. A. Koyi (2001), Estimating basal friction in accretionary wedges from the geometry and spacing of frontal faults, *Earth Planet. Sci. Lett.*, *194*(1–2), 221–227.

Schreurs, G., R. Hänni, and P. Vock (2001), Four-dimensional analysis of analog models: Experiments on transfer zones in fold and thrust belts, *Geol. Soc. Am. Mem.*, *193*, 179–190.

Simpson, G. (2011), Mechanics of non-critical fold–thrust belts based on finite element models, *Tectonophysics*, *499*(1–4), 142–155.

Sinclair, H. D. (1997), Flysch to molasse transition in peripheral foreland basins: The role of the passive margin versus slab breakoff, *Geology*, *25*(12), 1123–1126.

Sinclair, H. D., and P. A. Allen (1992), Vertical versus horizontal motions in the Alpine orogenic wedge: Stratigraphic response in the foreland basin, *Basin Res.*, *4*(3–4), 215–232.

Sommaruga, A. (1999), Décollement tectonics in the Jura forelandfold-and-thrust belt, *Mar. Pet. Geol.*, *16*(2), 111–134.

Spicher, A. (1980), *Tektonische Karte der Schweiz*, Bundesamt für Landestopographie, Bern.

Stampfli, G. M., G. D. Borel, W. Cavazza, J. Mosar, and P. A. Ziegler (2001), Palaeotectonic and palaeogeographic evolution of the western Tethys and PeriTethyan domain (IGCP Project 369), *Episodes*, *24*(4), 222–228.

Sue, C., B. Delacou, J. D. Champagnac, C. Allanic, P. Tricart, and M. Burkhard (2007), Extensional neotectonics around the bend of the Western/Central Alps: An overview, *Int. J. Earth Sci.*, *96*(6), 1101–1129.

Suppe, J. (2007), Absolute fault and crustal strength from wedge tapers, *Geology*, *35*(12), 1127–1130.

Süsstrunk, A. (1968), Erdstösse im Verzascatal beim Aufstau des Speicherbeckens, Vagorno, *Verh. Schweiz. Naturforsch. Ges.*, *1*, 89–92.

Thöny, W. (1999), A review of geochronological data from the Eastern Alps, *Schweiz. Mineral. Petrogr. Mitt.*, *79*, 209–230.

Trümpy, R. (1960), Paleotectonic evolution of the Central and Western Alps, *Geol. Soc. Am. Bull.*, *71*(6), 843–907.

Valley, B., and K. Evans (2009), Stress orientation to 5 km depth in the basement below Basel (Switzerland) from borehole failure analysis, *Swiss J. Geosci.*, *102*(3), 467–480.

Vollmayr, T., and A. Wendt (1987), Die Erdgasbohrung Entlebuch 1, ein Tiefenaufschluss am Alpennordrand, *Bull. Schweiz. Ver. Pet.-Geol. -Ingenieure*, *53*, 67–79.

von Hagke, C., C. E. Cederbom, O. Oncken, D. F. Stöckli, M. K. Rahn, and F. Schlunegger (2012), Linking the northern Alps with their foreland: The latest exhumation history resolved by low-temperature thermochronology, *Tectonics*, *31*, TC5010, doi:10.1029/2011TC003078.

Willett, S. D., and F. Schlunegger (2010), The last phase of deposition in the Swiss Molasse Basin: From foredeep to negative-alpha basin, *Basin Res.*, *22*(5), 623–639.

Williams, C. A., C. Connors, F. A. Dahlen, E. J. Price, and J. Suppe (1994), Effect of the brittle-ductile transition on the topography of compressive mountain belts on Earth and Venus, *J. Geophys. Res.*, *99*(B10), 19,947–19,974.

Yin, A. (1993), Mechanics of wedge-shaped fault blocks 1. An elastic solution for compressional wedges, *J. Geophys. Res.*, *98*(B8), 14,245–14,256.

Zoback, M. D., and J. Townend (2001), Implications of hydrostatic pore pressures and high crustal strength for the deformation of intraplate lithosphere, *Tectonophysics*, *336*(1–4), 19–30.